Thermally activated state transition technique for femto-Newton-level force measurement

Feng-Jung Chen,[1,2] Jhih-Sian Wong,[2] Ken Y. Hsu,[1] and Long Hsu[2,*]

[1]*Department of Photonics and Institute of Electro-Optical Engineering, National Chiao Tung University, 1001 University Road, Hsinchu 300, Taiwan*

[2]*Institute and Department of Electrophysics, National Chiao Tung University, 1001 University Road, Hsinchu 300, Taiwan*

**Corresponding author: long@cc.nctu.edu.tw*

Received December 15, 2011; revised February 17, 2012; accepted February 21, 2012; posted February 21, 2012 (Doc. ID 160071); published April 24, 2012

We develop and test a thermally activated state transition technique for ultraweak force measurement. As a force sensor, the technique was demonstrated on a classical Brownian bead immersed in water and restrained by a bistable optical trap. A femto-Newton-level flow force imposed on this sensor was measured by monitoring changes in the transition rates of the bead hopping between two energy states. The treatment of thermal disturbances as a requirement instead of a limiting factor is the major feature of the technique, and provides a new strategy by which to measure other ultraweak forces beyond the thermal noise limit. © 2012 Optical Society of America

OCIS codes: 120.3940, 120.4880, 170.4520, 350.4855.

State transitions are common occurrences in nature. Examples are state changes between the three phases of matter in physical processes, adhesion and detachment between cells [1], and the uncoiling and coiling of bacterial fimbriae in biomechanical phenomena [2]. Many chemical reactions also undergo state transitions [3]. The fundamental mechanism of such transitions is thought to be the underlying free energy state of matter, one of the important elements in statistical mechanics. In a pioneering study, Kramers postulated that a thermally activated state transition of a particle is analogous to transfer of the particle from one harmonic potential well to another [4]. Kramers' theory is universally accepted today [5]. Recently, the development of novel nanotechniques such as atomic force microscopy and use of optical tweezers [6] has inspired researchers to apply Kramers' theory to biomechanical processes, for example, to protein folding [7]. These theoretical works have tended to focus on modifying Kramers' formulas by adding the effect of an external force imposed on a biomolecule [8,9]. Application of one such model has provided new insights into the unfolding and folding pathways in the energy landscape of proteins from single-molecule mechanical unfolding experiments [10]. Despite widespread acceptance of the model, however, there have been few opportunities to test it quantitatively and fewer still to extend its application. In this letter we examine the model by means of a state transition system composed of a water-immersed Brownian bead in a bistable optical trap. We demonstrate that the state transition technique is a viable alternative to the optical spring-based photonic force microscope [11] and can measure comparable ultraweak forces.

Our thermally activated state transition system is shown in Fig. 1. A linearly polarized laser beam (1064 nm) was split into two laser beams by using a half-wave plate (HWP) and a polarized beam splitter (PBS). In Fig. 1, this is PBS1.The linearly polarized laser beams were coupled in the same way by two mirrors (M1 and M2) and by a second PBS (PBS2) and transformed to two mutually incoherent and circularly polarized beams by a quarter-wave plate (QWP). These transformed beams were then guided into an inverted microscope, and passed through an oil-immersed objective lens (OL, NA 1.25, Leica Microsystems) to form a bistable optical trap for the specimen. A silica bead (1 μm in diameter, 5% standard deviation) immersed in water and confined to the bistable trap was imaged on a high-speed charge-coupled device camera (CCD camera, GE680C, Prosilica Inc.) operating at 200 frames per second. The trapping height of the bead was controlled at 10 μm above a bottom coverslip. An asymmetric energy landscape of the confined bead was obtained by controlling the power ratio of the two beams. Changes in the energy landscape of the bead were produced by moving the specimen back and forth on a piezoelectric stage (P-561.3CD, Physik Instrumente), inducing a fluid flow force upon the bead. Data were only recorded and analyzed when the specimen moved to the left.

According to Kramers' theory, the transition rate of a classical Brownian particle from state A to state B (or from state B to state A) is

$$K_{A\to B(B\to A)} = K^0_{A\to B(B\to A)} \times \exp\{-[V_S - V_{A(B)}]/k_B T\}, \quad (1)$$

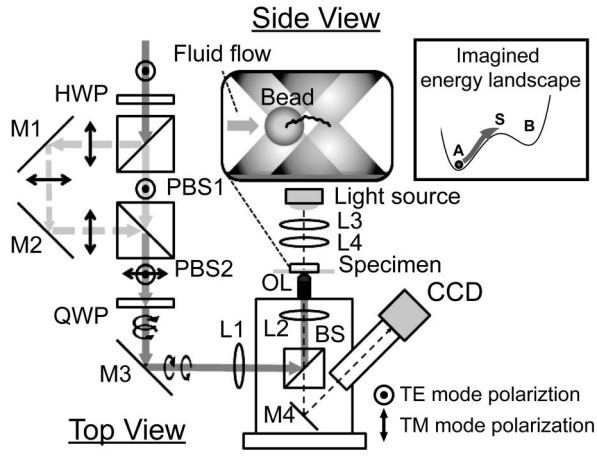

Fig. 1. Schematic diagram of the state transition system composed of a water-immersed bead in a bistable optical trap. Inset: an imagined energy landscape of the bead confined in the trap.

and the prefactor in an overdamped limit is

$$K^0_{A\to B(B\to A)} = \omega_S \times \omega_{A(B)}/2\pi\zeta, \tag{2}$$

where ω_S and $\omega_{A(B)}$ denote resonant angular frequencies surrounding the created transition barrier S and the state $A(B)$ of the particle, respectively, and ζ is the damping coefficient of the particle in its environment.

To incorporate the effect of a right-acting force F imposed on the particle of the state transition system, the forms of the transition rates are re-expressed as [8]

$$K_{A\to B} = K^0_{A\to B} \times \exp\{-[(V_S - V_A) - F \times \Delta x_{AS}]/k_B T\}, \tag{3}$$

$$K_{B\to A} = K^0_{B\to A} \times \exp\{-[(V_S - V_B) + F \times \Delta x_{SB}]/k_B T\}. \tag{4}$$

The symbols used in Eqs. (1–4) are shown in Fig. 2. Therefore, the individual transition rates of the particle from one state to another can be equalized by a specific force

$$F = (V_B - V_A)/\Delta x_{AB} \equiv F_{\text{eq}}, \tag{5}$$

provided that $K^0_{A\to B} \approx K^0_{B\to A}$.

The trajectory of a Brownian bead confined within the bistable optical trap can be tracked by digital imaging [12], a now-common method for tracking the nanometer-scale movements of a single fluorescent molecule [13]. The image process determines the centroid of every cross-correlation matrix derived from a sequence of recorded images and the image of the target bead. Figure 3(a) shows the trajectory of a bead confined to the bistable trap. The spatial probability density of the bead [Fig. 3(b)], estimated by sampling the trajectory distribution, follows a Boltzmann distribution $\rho(r) = \rho_0 \times \exp[-U(r)/k_B T]$. Here, $U(r)$ is the potential energy as a function of particle position, k_B is the Boltzmann constant (1.38×10^{-23} J/K), T was set to room temperature (298 K), and ρ_0 is a normalization constant. Therefore, the potential energy landscape of the optically-trapped bead can be derived directly from measurement, as shown in Fig. 3(c).

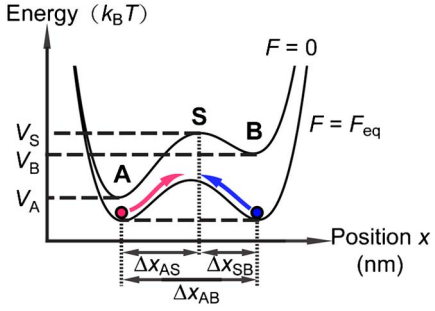

Fig. 2. (Color online) Energy landscape of two states A and B of a particle in the absence of a force and in the presence of a force F_{eq}, respectively. The symbol "S" represents a transition barrier.

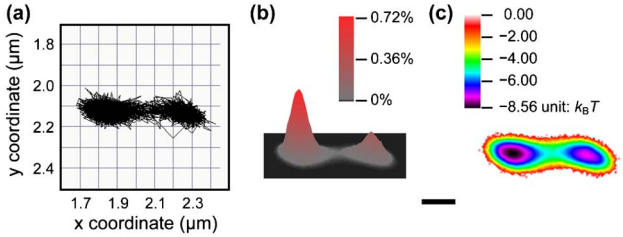

Fig. 3. (Color online) (a) Trajectory of a bead confined in the trap during 20 s (4000 frames), (b) spatial probability density of a bead with a spatial sampling of 10 nm is derived from the trajectory of the bead over 1 h (720,000 frames, oblique view), and (c) potential energy landscape of the bead is derived from panel b (top view). The scale bar for image sizes is 200 nm.

Figure 4 shows several experimentally determined energy landscapes of the same bead confined to the bistable trap under different flow force conditions. The flow forces were estimated from Stokes law, i.e., $F = \gamma \times v$, where the friction coefficient $\gamma = \zeta \times m = 3\pi\eta(T) \times d$ depends on the temperature-sensitive viscosity of water $\eta(T)$ and the diameter of the bead d. The symbol m represents the mass of the bead and v denotes the moving speed of the specimen. The speed was varied from 0 to 2 μm/s with a step of 0.5 μm/s. Corresponding Reynolds numbers were about 10^{-3}. The spacing of the two optical trapping points was precisely controlled at 760 ± 30 nm using the image process. The laser powers of left and right trapping beams were individually controlled at 31.1 and 27 mW before entry to the pupil of the objective. Consequently, the potential of the bead in state B was initially higher than that in state A. However, as the

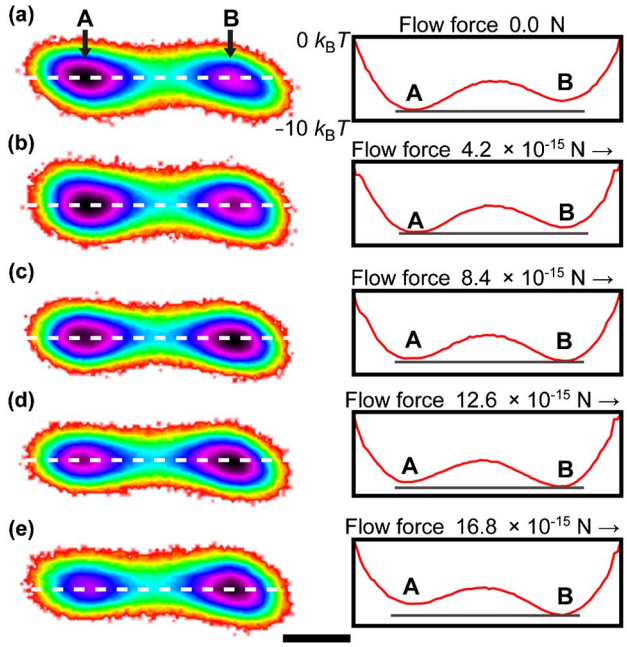

Fig. 4. (Color online) Experimentally determined energy landscapes of the same bead in the bistable trap and under a flow force of (a) 0 fN, (b) 4.2 fN, (c) 8.4 fN, (d) 12.6 fN, and (e) 16.8 fN. Left panel: two-dimensional energy landscape of the bead. Right panel: one-dimensional energy landscape as a function of particle position is derived from an energy level along a white dashed line in a corresponding left section. The scale bar is 200 nm.

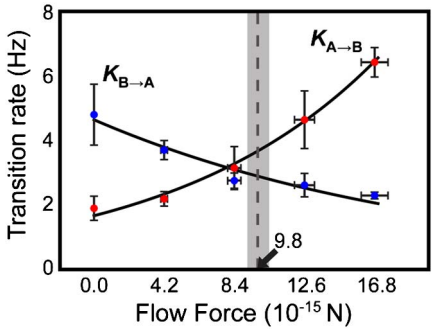

Fig. 5. (Color online) Two opposite changing behaviors of transition rates of the same bead as a function of increasing flow force. A force of 9.8×10^{-15} N is derived from Eq. (5). The gray bar represents the standard deviation region of the predicted force due to uncertainty of tracking positions. Because of additional error, the crossover point lies outside of the range admitted by position-tracking (see text for details).

flow force was increased beyond 8.4×10^{-15} N(fN), the potential level of the bead at state A became progressively higher than that at state B. Therefore, Fig. 4(c) represents the situation at which the two energies are equal. In addition, in Fig. 4(a), the potential energy difference between state B and state A is $1.025 k_B T$ and the spacing of the two states is 430 ± 30 nm. According to Eq. (5), the predicted equalizing flow force is 9.8 ± 0.7 fN. In addition, Eqs. (3) and (4) show that the change in a barrier height relative to state A as flow force increases is opposite to that relative to state B, suggesting that the two changes in transition rates of the bead are contrary to each other.

The transition rates of the same bead in Fig. 4 (defined as the inverse of the dwelling times of the bead in the two states) under different flow force conditions were calculated statistically, and are displayed graphically in Fig. 5. Because of the opposite changing behavior of the transition rates, the flow force can be approximated as the intersection of two exponential fitting curves obtained from Eqs. (3) and (4). This approach yields a flow force of ~8.0 fN. In addition, the prefactors were estimated to be similar ($K^0_{A\to B} \approx K^0_{B\to A} \approx 49$ Hz), suggesting that Eq. (5) is applicable to the experimental conditions. In practice, the specific flow force estimated from the transition rates and that predicted from Eq. (5) differ by a relative error of 22.5%. This error may be attributable to the inexact measurement and control of the environmental temperature T surrounding the system, uncertainty of the tracking positions (about 30 nm), and deviations in the bead diameter. Nonetheless, we have estimated the force F_{eq} within femto-Newton-level accuracy in the force sensor. An improvement to this estimate could be made by extending our analysis to three-dimensional energy landscapes [14].

Taking advantage of the sensitivity of thermal energy $k_B T$ and nanometer-precision control, the state transition technique emerges as a potentially excellent tool for the measurement of ultraweak forces (of the level of femto Newtons). The technique needs to rely on thermal disturbances, which can never be entirely eradicated, and which impede the performance of state-of-the-art techniques based on optical springs by limiting their force resolution [11,15]. Visual detection with micron-sized images in a bright-field microscope, which is simpler to implement than an optical trap-based technique with a nanometer-sized force probe [16], is another feature of the technique. However, a problem with this technique is its slow response to a transient force. Accurate ultraweak force measurements in our experiments required a recording duration of over 20 min. Whether the choice of a smaller bead trapped in this force sensor would have enabled faster force measurement remains to be confirmed.

To summarize, we have built an ultraweak force sensor composed of a Brownian bead immersed in water and restrained by a bistable optical trap. We have confirmed the modified Kramers' model and have shown that the state transition technique, based on the principles underlying the model, is capable of ultraweak force measurement beyond the thermal noise limit. The technique has here been tested only on femto-Newton-level flow forces imposed on the bead, but could be readily extended to study other types of forces, such as that induced by light [11,17] and the entropic force of DNA polymers [18]. By refining the model and/or introducing more precise experimental controls, measurement of forces down to sub-femto-Newton levels is foreseeable in the near future.

This study was supported by the National Science Council, Taiwan, Republic of China.

References

1. B. T. Marshall, M. Long, J. W. Piper, T. Yago, R. P. McEver, and C. Zhu, Nature **423**, 190 (2003).
2. F. J. Chen, C. H. Chan, Y. J. Huang, K. L. Liu, H. L. Peng, H. Y. Chang, G. G. Liou, T. R. Yew, C. H. Liu, K. Y. Hsu, and L. Hsu, J. Bacteriol. **193**, 1718 (2011).
3. R. F. Grote and J. T. Hynes, J. Chem. Phys. **73**, 2715 (1980).
4. H. A. Kramers, Physica (Amsterdam) **7**, 284 (1940).
5. P. Hänggi, P. Talkner, and M. Borkovec, Rev. Mod. Phys. **62**, 251 (1990).
6. W. J. Greenleaf, M. T. Woodside, and S. M. Block, Annu. Rev. Biophys. Biomol. Struct. **36**, 171 (2007).
7. R. Zwanzig, Proc. Natl. Acad. Sci. USA **94**, 148 (1997).
8. G. I. Bell, Science **200**, 618 (1978).
9. M. Andersson, E. Fällman, B. E. Uhlin, and O. Axner, Biophys. J. **90**, 1521 (2006).
10. I. Schwaiger, M. Schleicher, A. A. Noegel, and M. Rief, EMBO Rep. **6**, 46 (2005).
11. A. Rohrbach, Opt. Express **13**, 9695 (2005).
12. J. Gelles, B. J. Schnapp, and M. P. Sheetz, Nature **331**, 450 (1988).
13. M. K. Cheezum, W. F. Walker, and W. H. Guilford, Biophys. J. **81**, 2378 (2001).
14. L. I. McCann, M. Dykman, and B. Golding, Nature **402**, 785 (1999).
15. M. R. Pollard, S. W. Botchway, B. Chichkov, E. Freeman, R. N. J. Halsall, D. W. K. Jenkins, I. Loader, A. Ovsianikov, A. W. Parker, R. Stevens, R. Turchetta, A. D. Ward, and M. Towrie, New J. Phys. **12**, 113056 (2010).
16. O. M. Marago, P. H. Jones, F. Bonaccorso, V. Scardaci, P. G. Gucciardi, A. G. Rozhin, and A. C. Ferrari, Nano Lett. **8**, 3211 (2008).
17. F. Mueller, S. Heugel, and L. J. Wang, Opt. Lett. **33**, 539 (2008).
18. Y.-F. Chen, J. N. Milstein, and J. C. Meiners, Phys. Rev. Lett. **104**, 048301 (2010).